Structure, Vol. 11, 1413–1422, November, 2003, ©2003 Elsevier Science Ltd. All rights reserved. DOI 10.1016/j.str.2003.10.005

The Cyanide Degrading Nitrilase from *Pseudomonas stutzeri* AK61 Is a Two-Fold Symmetric, 14-Subunit Spiral

B.T. Sewell,*,[1] M.N. Berman,[1] P.R. Meyers,[2] D. Jandhyala,[3] and M.J. Benedik[3]
[1]Electron Microscope Unit
[2]Department of Molecular and Cell Biology
University of Cape Town
Private Bag, Rondebosch 7701
South Africa
[3]Department of Biology and Biochemistry
University of Houston
Houston, Texas 77204

Summary

The quaternary structure of the cyanide dihydratase from *Pseudomonas stutzeri* AK61 was determined by negative stain electron microscopy and three-dimensional reconstruction using the single particle technique. The structure is a spiral comprising 14 subunits with 2-fold symmetry. Interactions across the groove cause a decrease in the radius of the spiral at the ends and the resulting steric hindrance prevents the addition of further subunits. Similarity to two members of the nitrilase superfamily, the Nit domain of NitFhit and N-carbamyl-D-amino acid amidohydrolase, enabled the construction of a partial atomic model that could be unambiguously fitted to the stain envelope. The model suggests that interactions involving two significant insertions in the sequence relative to these structures leads to the left-handed spiral assembly.

Introduction

Enzymes from the nitrilase superfamily (Pace and Brenner, 2001) hydrolyze and condense a variety of nonpeptide carbon-nitrogen bonds utilizing a characteristic glu-cys-lys catalytic triad (Brenner, 2002). For this reason there is considerable interest in these enzymes as industrial catalysts (Cowan et al., 1998; Nagasawa and Yamada, 1989). Uses include the production of nicotinic acid, R−(−)−mandelic acid, S−(+)−ibuprofen and the detoxification of cyanide waste.

A number of enzymes whose ability to degrade or modify cyanide have been described. Within the superfamily, nitrilases are the group of enzymes that hydrolyze nitriles (R-C ≡N) (of which cyanide [HCN] is the simplest) to ammonia and the corresponding carboxylic acid (RCOOH) (Pace and Brenner, 2001), whereas nitrile hydratases hydrolyze nitriles to the corresponding amide. Cyanide degrading enzymes can be of two types. The first group, the cyanide dihydratases, comprise a group of bacterial enzymes that include those from *Alcaligenes xylosoxidans* subsp. *denitrificans* DF3, *Bacillus pumilus* C1, and *Pseudomonas stutzeri* AK61 (Ingvorsen et al., 1991; Meyers et al., 1993; Watanabe et al., 1998a). All these behave as true nitrilases, converting cyanide directly to formate and ammonia. The enzymes in another group, the cyanide hydratases, which hydrolyze cyanide to formamide, are all of fungal origin. These enzymes are more closely related to the nitrilases and should not be confused with the unrelated metal-containing nitrile hydratases (Pace and Brenner, 2001). The best characterized cyanide hydratases are those from *Fusarium lateritium* and *Gloeocercospora sorghi* (Cluness et al., 1993; Wang et al., 1992).

The enzyme from *P. stutzeri* discussed here is a cyanide dihydratase that catalyzes the reaction $HCN + 2H_2O \rightarrow NH_3 + HCOOH$. The organism was isolated from the effluent of a metal plating plant and was selected for its ability to grow in 1 mM KCN as a possible agent for the bioremediation of cyanide spills (Watanabe et al., 1998b).

The role of the nitrilases in the cellular context is not generally well characterized except in the case of *Arabidopsis thaliana* (Bartling et al., 1994), where a nitrilase converts 3-indolylacetonitrile to the hormone auxin (3-indolylacetic acid).

Pace and Brenner (2001) list the sequences of 176 enzymes in the nitrilase superfamily obtained by multiple PSI-BLAST searches. Their analysis classified sequences in the nitrilase superfamily into 13 branches. At the time of publication, the nitrilase branch contained 25 members from 17 organisms. Twelve other branches of the nitrilase superfamily encode amidases, protein N-terminal acyltransferases, or predicted amidases of varying specificities. Crystal structures of NitFhit (Pace et al., 2000) and N-carbamyl-D-amino acid amidohydrolase (Nakai et al., 2000), which are members of two other branches of the nitrilase superfamily, show that these enzymes form tetramers with 222 symmetry. Pace et al. (2000) have described a naturally occurring fusion protein in *Caenorhabditis elegans* in which a nitrilase homolog, Nit, is fused to an enzyme known to be crucial in apoptosis, Fhit. The fusion of the two enzymes is proposed to imply a functional, but as yet unknown, link of two separate pathways. DCase (N-carbamyl-D-amino acid amidohydrolase) (Nakai et al., 2000) catalyzes the hydrolysis of N-carbamyl-D-amino acids to the corresponding D-amino acids and is predicted to be a nitrilase homolog.

Determination of subunit size by SDS-PAGE or sequencing and complex size by gel filtration, light scattering, or electron microscopy suggest that several of the nitrilases are homooligomers with subunit numbers varying from 10 to 18 in different cases, whereas the fungal cyanide hydratases form complexes of several megadaltons. In particular, the molecular masses of nitrilases from *Bacillus pallidus* (Almatawah et al., 1999), *Rhodococcus rhodochrous* K22 (Kobayashi et al., 1990, 1992), *Fusarium oxysporum* f. sp. *melonis* (Goldlust and Bohak, 1989), and *Acinetobacter* sp. AK 226 (Yamamoto and Komatsu, 1991) suggest that these enzymes are 14-mers. Certain members of the family are reported to occur as monomers or dimers. However, upon incubation with substrate, the dimers of the enzyme from *R.*

*Correspondence: sewell@uctvms.uct.ac.za

rhodochrous J1 were observed to form a decamer (Nagasawa et al., 2000). The monomeric nitrilases from *Rhodococcus* sp. NCIB 11216 (Harper, 1976, 1977) and *Rhodococcus* sp. ATCC 39484 (Stevenson et al., 1992) also associate to form dodecamers on incubation with substrates or inhibitors. The nitrilase from *Klebsiella ozaenae* (Stalker et al., 1988) appears to be an exception to this rule. Even though it has considerable sequence homology to the others, it is reported to remain a dimer.

In this paper we report on the use of three-dimensional electron microscopy and homology modeling to provide the first detailed interpretation of the quaternary structure of one of these economically important enzymes. The enzyme complex is shown to be a 14-subunit spiral in which four interactions occur across the groove. Fitting a dimer model based on the known structures of members of the nitrilase superfamily leads to an interpretation of the structure and identifies widespread insertions in sequence relative to the known structures as being the site of interaction leading to spiral formation. A model for the termination and hence variability in the number of subunits found in these enzymes based on steric hindrance caused by the interactions across the groove and allowed by the flexibility of the newly identified interface is proposed.

Results

Structural Alignment and Homology Modeling

A search for structural alignment using three of the nitrilase sequences, namely those from *P. stutzeri*, *B. pumilus* C1 and *G. sorghi*, against solved structures in the PDB using GenTHREADER (Jones, 1999a) produced two candidates which scored higher than 0.98 against all three, namely DCase (accession number 1erz) (Nakai et al., 2000) and the Nit domain of NitFhit (accession number 1ems) (Pace et al., 2000). The identity between the nitrilase sequences and those of the solved structures was less than 20%. The alignments, as predicted by GenTHREADER and slightly modified by hand, are shown in Figure 1.

Alignment of DCase and the Nit domain using ALIGN (Cohen, 1997) showed that the structure of the central core of β sheets and the region including the three active site residues was well conserved with 111 α carbon atoms matching to within 1.5 Å. α carbon locations in the two interacting surfaces and the α helix (NH5) following the β loop which forms the B surface (described below) are also well conserved. Structural variability was contained in five externally located regions, three of which are β loops and two of which are near externally located helices. *P. stutzeri* nitrilase has two major insertions relative to the Nit domain, 1 of 13 amino acids immediately prior to a region of α helix (NH2) beginning at residue lysine 63 in the Nit numbering, and 1 of 14 amino acids effectively lengthening the β loop between residues asparagine 229 and arginine 232 in the Nit numbering (NS9 and NS10). Deletions of residues 99–102, 133–140, and 197–201 are all in external loops. The structure in the region following residue 63 is not well conserved between Nit and DCase, being an α helix in Nit and a meandering coil in DCase. Prediction of the *P. stutzeri* nitrilase secondary structure using PSIPRED (Jones, 1999b) suggests that this region is α-helical. There are no insertions or deletions in the regions in which there is good structure conservation between Nit and DCase. Another significant difference is that *P. stutzeri* nitrilase has 38 more C-terminal amino acids than DCase. Comparable features including the regions of good conservation, the insertions and deletions in the external loops, and the C-terminal extension are also found in the sequences of the cyanide degrading nitrilases of *B. pumilus* C1 and *G. sorghi*, both of which are known to form spiral structures (Jandhyala et al., 2003; Price et al., 2002).

An initial model of the monomer of the *P. stutzeri* nitrilase was made by substituting the side chains of *P. stutzeri* into the structure of the A chain of Nit using SCWRL (Bower et al., 1997) according to the alignment shown in Figure 1. In the initial model no attempt was made to model the insertions after residues 62 and 229 or the C-terminal extension.

The map of the of *P. stutzeri* nitrilase (described below) has a global 2-fold axis which must coincide with a dimer axis. This suggests that it would be more appropriate to use a dimer model rather than a monomer model to fit the map. The decision on how to construct this dimer model was based on an analysis of the crystal structures. Both the Nit domain and DCase are found in crystals as tetramers having 222 symmetry. The two contact surfaces, which we will refer to as surface A and surface B, are located almost perpendicular to one another (Figure 2A). Surface A comprises three α helices in DCase (α5, α6, and α8) or two α helices and a length of β sheet in Nit (NH3, NH4, and NS13) such that the αββα sandwich becomes an αββααββα superstructure. In both cases the helices α6 cross near their middle at an angle of about 70°, while the helices α5 cross near their end at an angle of about 15°. Surface B comprises the two strands of sheet (β13 and β14) at the edges of the two central sheets of the αββα sandwich. Each of these strands runs antiparallel to the strand in the neighboring subunit and hydrogen bonds are formed down most of their length. This has the effect of extending the central sheets over both pairs of the dimer. The correspondence between α carbon positions between Nit and DCase is as good in the case of the helices in surface A and the sheets in surface B as it is in the central core (i.e., less than 1.5 Å between corresponding positions). The correspondence in the final element of surface A, designated NS13 in Nit and α8 in DCase, is poor.

Pace et al. (2000) reported substantial sequence conservation in the A surface that they predicted would be conserved in all Nit proteins and expressed some doubt about the widespread preservation of the B surface owing to the lack of conservation of certain ion pairs in vertebrate and fungal Nit proteins. These considerations, together with the possibility that additional interactions arising from the C-terminal extension could also contribute to the A surface, would seem to favor an initial dimer model in which this surface is preserved (Figure 2B).

The Three-Dimensional Map

The resolution of the final map, on which 2-fold symmetry was imposed, was 2.5 nm, corresponding to the point

Figure 1. Alignment of Sequences

Alignment of the sequences of the cyanide dihydratases from *B. pumilus* C1 (Bpum), *P. stutzeri* AK61 (Pstu), and the cyanide hydratase from *G. sorghi* (Gsor) with those of the two related crystallographically determined structures, N-carbamyl-D-amino acid amidohydrolase (DCase) from *Agrobacterium* sp. strain KNK712 (Nakai et al., 2000) and the Nit domain of NitFhit from *C. elegans* (Nit) (Pace et al., 2000).
The alignments of Nit and DCase are based on their structures and are presented in JOY notation (Mizuguchi et al., 1998). Regions of substantial structural conservation are highlighted in yellow and the three active site residues, numbered E54, K127, and C169 in Nit numbering are highlighted in pink. The external loops in which the cyanide degrading nitrilases have substantial insertions or deletions are highlighted in brown. The contact surfaces A (highlighted in green) and B (highlighted in blue) in Nit and DCase are described in the text. The notation used to describe the elements of secondary structure in DCase and Nit is given below the alignment.

at which the value of the Fourier shell correlation of two structures generated from different halves of the image set was 0.5. The map (Figure 3) reveals the structure to be a spiral with a length of 18 nm and a diameter of 12 nm having 1.67 turns and a pitch of approximately 8.5 nm. The radius of the spiral is greater at the center than at the ends by about 1 nm. At high contour levels, there are 14 discrete density peaks and therefore the molecular envelope was set at 730 nm^3 corresponding to the volume occupied by 14 subunits of molecular weight 38 kDa (Watanabe et al., 1998a). The overall structure has a 2-fold axis passing through its center relating subunits A–G to subunits H–N (Figure 4A). The handedness of the spiral was not determined a priori, but it is shown as left-handed based on evidence presented below.

A cylindrical projection of the map (Figure 4B) enabled the angular displacements between the repeating motifs to be measured. The rotations measured to the apparent positions of the local pseudo-2-fold axes are ±71°, ±147°, and ±244°, respectively. These angles were refined on model fitting to ±71°, ±149°, and ±234°. Between these locations there are also local pseudo-2-fold axes of a different kind, indicating the presence of a separate intersubunit interface. Displacements of the motifs along the helix axis appeared to be fairly constant at 1.6 nm. These displacements were also refined on model fitting as can be seen from Table 1. The projections of the motifs toward the end of the helix appear elongated because they are closer to the helix axis.

Features of the map of interest include the following: a pronounced bulge on the inside of the spiral coinciding with the overall 2-fold axis and at corresponding local dyad locations (red surfaces in Figure 4A), a ridge on the outside of the spiral at each of other local dyad positions (orange surfaces in Figure 4A), and four contact points across the groove, labeled a, b, c, and d (Figures 3 and 4A).

Interpretation of the Map

The three-dimensional map of the negatively stained cyanide dihydratase has a number of features that aid in its interpretation by allowing the model generated above to be placed in the experimentally determined density. As can be seen from the view of the complex shown in Figure 3C, the dyad axis of the complex coincides with the dyad axis of a dimer.

It is postulated that either one or other of the associating surfaces found in Nit and DCase are preserved in

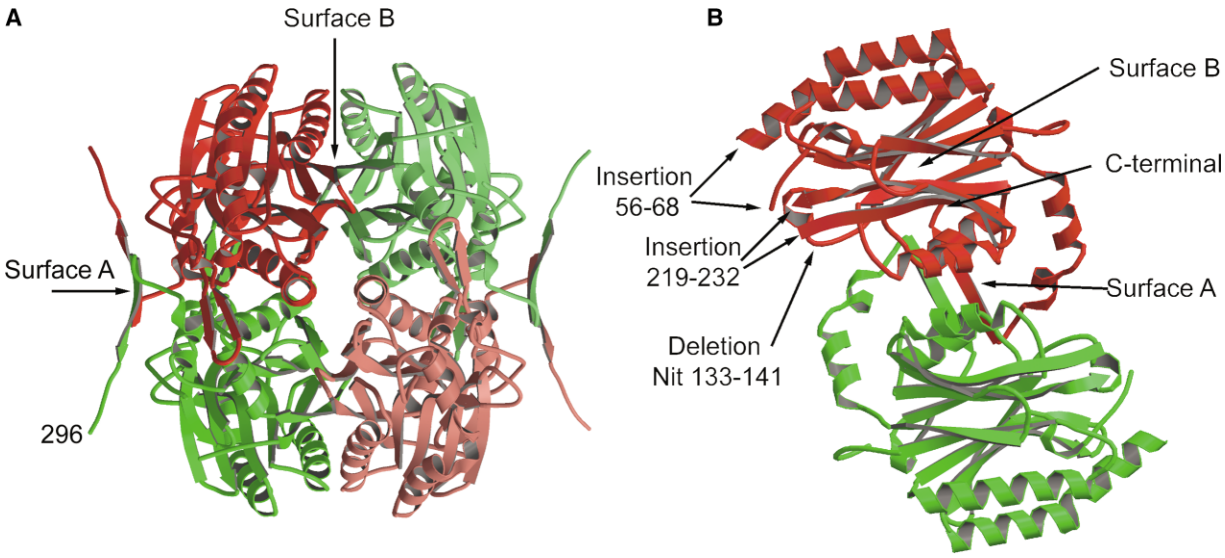

Figure 2. Tetramer of the Nit Domain and Dimer Model of *P. stutzeri* Nitrilase

(A) Tetramer of the Nit domain of NitFhit showing the two interacting surfaces described in the text.

(B) Dimer model of *P. stutzeri* nitrilase used to locate the molecules in the map. No attempt was made to model the structure of the two significant insertions whose location is indicated. The location of one significant deletion relative to the Nit structure (referred to in the text) is indicated.

the complex. This gives rise to four possibilities for fitting a model of the dimer into the density which must be fitted into maps of each handedness. It was not immediately obvious from fitting the density which of the two possibilities (A or B surface preserved) is correct. However, the curvature of the density suggests clear preferences for the location of the inner and outer surfaces with respect to the spiral axis in both cases. A preliminary model of the spiral structure was created by applying the transformations that had been measured from the cylindrical plot to a dimer that had been aligned to the dyad axis and refining the fit manually using O (Jones et al., 1991).

Models built on the basis of dimerization around the B surface were rejected for three reasons: (1) the failure to find a reasonable explanation for unfilled regions of density, notably the bulge on the inner surface of the spiral, (2) a clash at the C-terminal region involving NH5 and NS13 and NH3 of the neighboring molecule in the quaternary spiral, and (3) a number of instances in which the model structure is not contained within the negative stain envelope.

The initial model (omitting the insertions relative to Nit) built on the basis of dimers formed around the A surface, as shown in Figure 2B, fitted the density better. In particular, a bulge on the 2-fold axis on the inner surface of the spiral (Figure 5B) was filled by a structural feature corresponding to NS13 in the NitFhit structure at the C-terminal end of the Nit domain.

Automatic fitting of the model to the density using SITUS both confirmed the locations of the dimers and enabled them to be located in the density with greater precision than direct measurement from the cylindrical projection or hand fitting (Figure 5A). Useful parameters measured from the fitting include the relative locations of the centroids of the dimers and the relative tilt of the

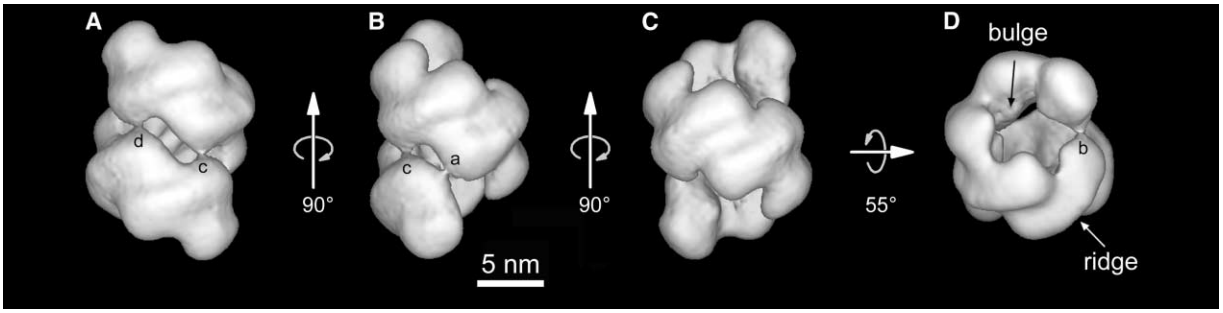

Figure 3. Views of the Map Contoured so as to Enclose a Surface of 730 nm^3

The axis of the spiral is vertical and the relationship between the views (A)–(D) is indicated. The global 2-fold axis is apparent in views (A) and (C) which are viewed along (−1,0,0) and (1,0,0) respectively. The complex is a short spiral segment of 1.67 turns. The inner radius of the molecular envelope is 1.8 nm for the central subunits and the outer radius is 6.2 nm compared to an inner radius of 0.9 nm and an outer radius of 5.1 nm for the end subunits. Features of the map referred to in the text are labeled.

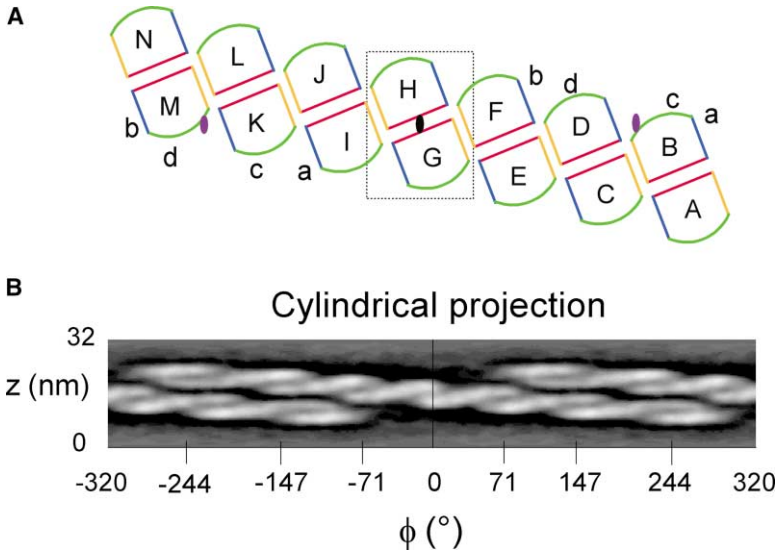

Figure 4. Schematic Diagram of the Subunit Locations and Cylindrical Projection of the Map

(A) Schematic diagram of the subunit locations in the unwound spiral. The location of the global dyad is indicated. The G and H subunits (outlined) are related by the global dyad. Subunit associations across the surfaces depicted as red and orange result in local pseudo dyad symmetry at these interfaces. The contact points between subunits in successive turns of the spiral are labeled a, b, c, and d.

(B) An extended cylindrical projection of the map spanning 640° in order to show the spiral as continuous density. The angular displacement of the global dyad axis is indicated as 0° and the displacements of the corresponding (i.e., red surface) local pseudo-dyad axes are indicated on the ϕ axis. The angular displacement of successive dyad axes increases toward the extremities, the successive displacements measured from the projection being 71°, 76°, and 97°. The projections further from the global dyad span an increasing angular range, resulting in their appearance becoming more elongated. This is because the subunits are closer to the helix axis.

dimers (Table 1). The fitting confirms the 1 nm decrease in the diameter of the spiral from the center to the ends. Fits to both left-handed and right-handed maps were performed. Correlation coefficients for dimers EF, GH, and IJ (which are best defined) were 5% higher in the case of left-handed maps than right-handed maps.

Our fitting confirms that the A surface is mating across the global dyad axis and enables the orientation of the dimer to be determined by locating the density corresponding to NS13 in the bulge on the inside of the quaternary spiral. It is not surprising that the primary structural component should be a dimer built around the A surface as it is more extensive than the B surface. Both the secondary structure prediction and the local topology suggest that a model of the NS13 region based on NitFhit is more appropriate to our case than one based on DCase, in which this region is helical.

The model polypeptide emerges from the density envelope at the amino acid corresponding to residue 291 in the NitFhit sequence, at the bulge. There is no clearly defined density to accommodate the remaining 38 C-terminal amino acids. This may be because flexibility in this region results in a lower average density.

The remaining density which was unfilled by the initial model is the ridge between the dimers and on the outside of the spiral in what would correspond to the orange surface in the schematic diagram (Figure 4A). In the case of a left-handed spiral, both of the major insertions relative to Nit (i.e., residues 56–68 and residues 219–232 in the *P. stutzeri* numbering) point directly into this density, which is located on a local pseudo-2-fold axis. This is a most satisfactory result, providing at once an explanation for the experimentally observed density and for the formation of the spiral, which must be due to interaction between these regions that are absent in the two crystallographically determined proteins. A similarly satisfying explanation for either the density or the location of the insertions does not occur in the case of a right-handed spiral.

Table 1. Cylindrical Polar Coordinates of the Centroids of Dimers in the Spiral and the Tilts of Their Dyad Axes Toward the Axis of the Spiral

Dimer	r (nm)	ϕ(°)	z (nm)	Tilt (°)
AB	3.15	234	−5.08	12
CD	3.70	149	−3.21	4
EF	4.12	71	−1.35	1
GH	4.20	0	0.00	0
IJ	4.13	−71	1.35	−1
KL	3.70	−149	3.21	−4
MN	3.14	−234	5.09	−12

The location of the centroids of each dimer are given in cylindrical polar coordinates. The global dyad axis is located along $\phi = 0°$ in the plane z = 0. The tilt of the local dyad axis of each dimer relative to this plane is indicated.

Intersubunit Contacts

Contacts between the subunits occur along the length of the helix primarily at two surfaces shown as red and orange in the schematic diagram shown in Figure 4A. One of the contacts, across the red surface, coincides with the global 2-fold axis. This corresponds to the A surface. All the other contacts along the helix length across both orange and red surfaces appear to have local pseudo-dyad symmetry. The surface depicted in orange is not present in the NitFhit structure and is proposed to arise due to interactions between the amino acids in the two significant insertions which are described above. We will call this the C surface.

Modeling also suggests that there is a contact between the surfaces depicted as red and green. There are four additional contacts between subunits across

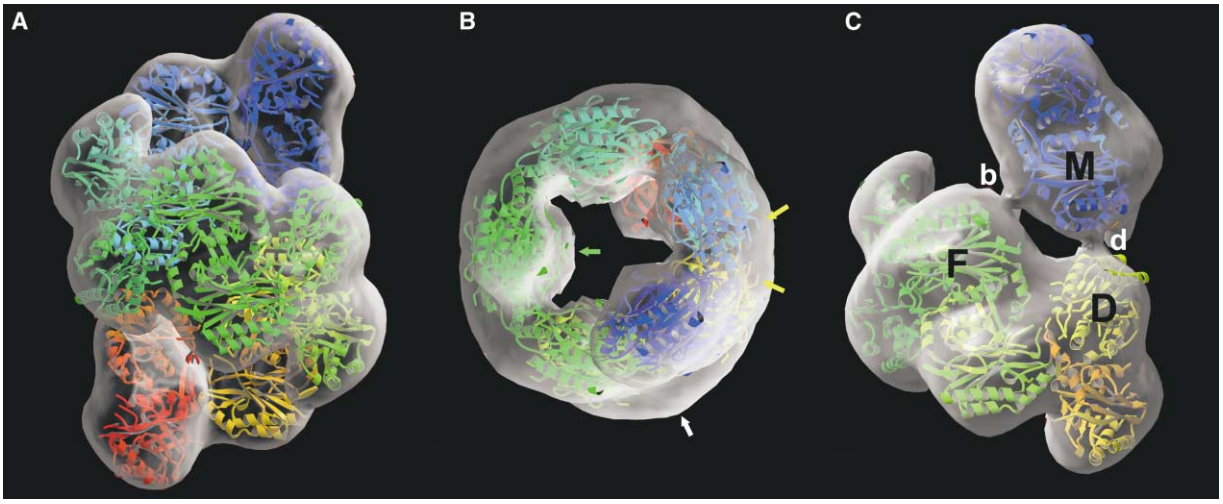

Figure 5. Fourteen Subunits Fitted to the Density

(A and B) Subunits viewed parallel to the global 2-fold axis (A) and parallel to the axis of the spiral showing the ridge of unfilled density (white arrow) between the subunits (B). The subunits depicted are those used in the SITUS fitting in which the significant insertions (53–65 and 219–233) are missing. The ends of the β sheet (residues 219 and 233) can be seen pointing into the vacant density (yellow arrows). The bulge accommodating the region corresponding to NS13 in Nit can also be seen on the inside surface of the spiral (green arrow).

(C) The tilt of the MN terminal dimer which occurs as a result of the interaction at point b. In this view the rear half of the complex has been removed by clipping in the plane of the global dyad.

the groove at the points labeled a, b, c, and d that are a result of the spiral quaternary structure. The contacts a (between subunits B and I) and b (between subunits F and M) are near the end of the helix NH2 and appear not to have local symmetry, whereas the contacts c (between subunits B and K) and d (between subunits D and M) are located near the middle of helix NH2 and appear to have local 2-fold pseudo symmetry.

The deletion of residues 133–141 (Nit numbering), which is a protruding β loop in Nit, is essential to allow the interactions at the C surface. These amino acids are also deleted in the nitrilases from *B. pumilus* C1 and *G. sorghi*. The deletion at 197–201 is interesting as this will either have the effect of shortening a conserved internal strand of β sheet (NS7 in Nit) or altering the length of the long helical segment (NH3 in Nit) involved in surface A, or a combination of both. In Nit, the amino-terminal side of NH3 plays a role in determining the direction of the strands NS9 and NS10, which are the locations of the putative β sheet insertion in the *P. stutzeri* nitrilase. Removing this support increases the range of structures that can be adopted by the insertion, possibly contributing to the flexibility of the interface formed by the C surface.

Termination of the Spiral

Table 1 indicates two factors that could conceivably lead to the termination of the spiral. The first is the decrease in radius and the other is the increase in tilt of the subunits. It should be noted that the terminal dimers tilt inward, toward the axis of the spiral, by a rigid body rotation of 12°. This tilt presumably comes about as a result of the interactions at points a and b (Figure 5C). As a result of both of these factors, insufficient space is available to accommodate another subunit and continue the spiral.

Discussion

Quaternary structure of the type observed in the nitrilase from *P. stutzeri* AK61 has been previously reported by us to occur in the case of the homologous nitrilase from *B. pumilus* C1 (Jandhyala et al., 2003). It comprises a defined length, 2-fold symmetric, one start spiral, in which the subunits interact across two surfaces. The clarity of the map reported here enables an interpretation of the structure by homology modeling and suggests an explanation for the termination of the spiral.

Homology modeling based on the two crystal structures of the members of the superfamily enables the construction of a dimer model which can be unambiguously located in the experimentally determined molecular envelope. The envelope also contains unfilled space between the dimers which, only in the case of a left-handed spiral, can be filled by residues from the two substantial insertions relative to the two solved structures (residue numbers 56–68 and 219–232). The structure suggests local pseudo dyad symmetry across this interface and we therefore propose that residues contributed by the insertions interact across this interface, which we call the C surface (indicated in orange in Figure 4A) leading to the spiral assembly. Residues 219–232 are an insertion at the end of a β loop and could conceivably continue the loop. If this were the case, the 2-fold symmetry of the interface could produce a four-stranded antiparallel β sheet straddling the subunits.

It can be deduced from Table 1 that the environment of each non symmetry related subunit within the complex is slightly different suggesting that there is some variability in the interactions between the subunits. This may occur due to the flexibility of the loops and the interactions between them. Such flexibility would give rise to a hinge, which would enable local optimization of interactions

as new possibilities arose due to the changed environment of each subunit as the spiral elongates.

In particular, as subunits are added at the terminus of the spiral, new opportunities arise for interactions across the groove after the formation of a single turn. The continuation of the spiral by the addition of a further subunit will occur if the energetic considerations favor this in preference to interactions across the groove which distort the helical symmetry, resulting in steric hindrance and thus preventing the addition of a further subunit. Observed deviations from perfect helical symmetry result in a structure that is narrower at the ends and that has an inwards tilt of the terminal dimer, suggesting that this is the mechanism for the termination of the spiral.

It is predicted that the geometry imposed by the various interactions will determine the number of subunits that can be added to the spiral and hence the overall length. The majority of the nitrilases described to date are homooligomers of 10–18 subunits. This raises the question whether the principles underlying the quaternary structure in these cases are similar to those in the nitrilase from *P. stutzeri*. The variety of reported molecular weights may indicate that the different complexes have different, but specific, numbers of subunits that could be assembled in a truncated spiral form. The fungal cyanide hydratase, with a reported molecular weight of up to 10 MDa (Fry and Munch, 1975) would be the extreme case of an open, regular helix (Price et al., 2002) that does not terminate at a specific length. We have previously (Jandhyala et al., 2003) reported a pH-dependent transition in the case of the *B. pumilus* C1 enzyme in which the 18 subunit spiral occurring at the optimum pH (pH 8) becomes a regular open helix at pH 5.4. This behavior, which could result from the change in charge on a histidine (pKa = 6.05), supports the notion of the optimization of interactions across the groove and the idea of a flexible hinge.

The 2-fold symmetry of the complex imposes the limitation that the number of subunits in each complex is an even number. Interactions between subunits occur predominantly at the A and C surfaces. In any particular enzyme, interactions across either one of these interfaces may be preferred. In those cases in which the A surface interactions are stronger, for example, this imposes the further restriction on the number of subunits that would occur in spiral structures. Following our model, the minimum number of subunits required to complete a single turn would be 10 subunits. Successively adding dimers at either end would result in spirals with 14, 18, 22, etc. subunits. Details of structure, including the flexibility of the C surface and the possibilities for interaction between subunits across the groove would determine the point at which the spiral terminated in each case. However, the deviation from regularly repetitive helical symmetry operators in the case of structures with 22 or more subunits (thus completing more than two turns) would be so small that it is likely that these would form regular, open helices.

Our assertion that the spiral is left-handed was at first based on the slightly better correlations of our initial dimer model to the left-handed version of the map. Our confidence in the left-handed model is enhanced by our experimental determination of the hand of the extended helices of the similar nitrilase from *B. pumilus* C1 by heavy metal shadowing (Jandhyala et al., 2003) and the fact that this fitting gives a reasonable interpretation for the unfilled density in terms of the insertions relative to the Nit sequence. Indeed, the location of the insertions in the model provides compelling evidence that the spiral is left-handed, leading, as it does, to a consistent explanation for the formation of the spiral structure.

The location of the α helix corresponding to NH2 in Nit in our model suggests that interactions between amino acids in this region play a role in stabilizing the quaternary structure through the interacting points labeled c and d in Figure 3. Amino acids near the N-terminal end of NH2 are also probably responsible for one side of the asymmetric interactions labeled a and b—the other side being in the region of the loop between NS5 and NS6. These interactions may be responsible for distorting the helix and driving the structural changes that result in helix termination. Attempts to locate the actual residues involved in these interactions are speculative in a map of this resolution.

The active site, based on similarity with enzymes in the nitrilase superfamily (Pace et al., 2000; Nakai et al., 2000), comprises the residues glutamic acid 47, lysine 129, and cysteine 163 in the *P. stutzeri* numbering. In our model, the active site is located so that substrate would have access to it from the outside of the quaternary spiral. Substrate would have to approach the spiral at an oblique angle and would reach the active site through a narrow opening between the A and C surfaces. An immediate question which arises is whether the quaternary structure has any influence on the enzyme activity. In the case of the *P. stutzeri* nitrilase, the enzyme has always been studied with the quaternary structure intact. However, the homologous nitrilases from *R. rhodochrous* J1, *Rhodococcus* sp. ATCC 39484, and *Rhodococcus* sp. NCIB 11216 have been isolated as dimers or monomers, which are inactive against the aliphatic substrates such as acrylonitrile, but can be induced to form the active decameric or dodecameric complex by preincubation with the substrate, benzonitrile (Harper, 1976, 1977; Stevenson et al., 1992; Nagasawa et al., 2000). This raises the possibility that conformational change induced by ligand binding at least enhances the activity toward certain substrates. It is conceivable that strain induced by substrate binding alters the conformation to encourage association and that additional strains induced by the higher order aggregation alter the active site conformation to produce activity or alter substrate binding. The details of the influence of the higher order associations on the activity and substrate specificity of *P. stutzeri* nitrilase require further investigation.

The B surface, comprising the edges of sheets NS11 and NS12, is exposed on the outside of the quaternary spiral. The unpaired hydrogen bonds on the sides of the loop could form a "sticky patch," possibly enabling another protein to dock at this position and form a larger complex. Insight into the need for such an arrangement could be gained from an understanding of the biological role of these enzymes, which is currently poorly understood.

Biological Implications

The 3D structures of NitFhit (Pace et al., 2000) and N-carbamyl-D-amino acid amidohydrolase (Nakai et al., 2000) established that two divergent members of the nitrilase superfamily (Pace and Brenner, 2001) are 222 tetramers and suggested that one of the two dimer interfaces is likely to be conserved in the superfamily (Pace et al., 2000). Nonetheless, the apparent native sizes of nitrilases have ranged from reports of monomers (Harper, 1977; Stevenson et al., 1992; Bhalla et al., 1992) and dimers (Stalker et al., 1988; Nagasawa et al., 2000) to tens (Ingvorsen et al., 1991; Watanabe et al., 1998b; Jandhyala et al., 2003; Almatawah et al., 1999; Kobayashi et al., 1990; Yamamoto and Komatsu, 1991; Goldlust and Bohak, 1989) or hundreds (Cluness et al., 1993; Wang et al., 1992) of subunits.

By fitting Nit-homologous dimers of nitrilase into the experimentally determined left-handed spiral structure, we show that the cyanide dihydratase of *Pseudomonas stutzeri* AK61 is a 14-mer and propose a basis for the assembly of smaller and larger 2-fold symmetric oligomers of these enzymes.

This involves a new quaternary structural principle in which subunits associate to form a spiral of limited length. In this structure, each pair of 2-fold related subunits adopts a different conformation thought to be dictated by local minimization of energy involving interactions which occur across the groove as the length of the spiral exceeds one turn. Conformational differences are postulated to be allowed by a flexibility in the interface between the subunits. Limitation of the length results from steric hindrance that prevents the addition of further subunits as distortions in the spiral arise due to the interactions that occur across the groove.

The other known limited length homooligomeric spiral structure, namely tripeptidyl peptidase II from *Drosophila* (Rockel et al., 2002), is a completely different two start helical arrangement and thus requires a different explanation for its termination.

The sequences of several cyanide degrading enzymes, as well other nitrilases, suggest a high level of structural homology. Two significant insertions in the sequence relative to members of the superfamily which have known structures are proposed to be the site of interaction leading to the spiral assembly. These insertions, which have variable sequence, are present in all known bacterial and fungal nitrilases (including homologous cyanide hydratases), suggesting that the principles described here are common to these enzymes.

The enzyme described here is known to hydrolyze cyanide, but specific evidence that this is its natural substrate in the cell is lacking. Given this lack of information, it is difficult to speculate on the significance of the quaternary structure. However, in the case of the nitrilases from three *Rhodococcus* species, preincubation with a substrate leads to the formation of oligomers that assume activity in the assembled state, suggesting an interplay between the quaternary structure and the active site. Other potential consequences of the structure include the concentration of enzyme active sites in one cellular location and the possibility of building a larger complex involving other enzymes, which may be involved in the same pathway.

Experimental Procedures

Expression and Purification of Cyanide Dihydratase from MB2784 Cells

E. coli MB2784 cells, i.e., *E. coli* BL21(DE3)pLysS cells transformed with a pET26b expression plasmid (Novagen) containing the nitrilase gene from *P. stutzeri* AK61, were grown at 37°C in Luria broth containing 30 μg/ml kanamycin to OD_{600} = 0.9. IPTG was added to 1 mM. Cells were harvested after allowing growth for a further 9.75 hr to a final density of OD_{600} = 3.35.

The cells were then washed twice in cold 10 mM Tris, 50 mM NaCl (pH 8), and resuspended in 1/40 volume of the same buffer containing 1 mM EDTA, 0.5 μg/ml leupeptin, and 2 μg/ml aprotinin. The cells were ruptured by sonication for 5 min, with pauses for cooling, in a Virsonic Digital 475 Ultrasonicator (Virtis, USA) using a blunt, 0.5 inch horn. This and all subsequent steps were performed at 4°C.

The lysate was centrifuged for 1 hr in a Beckman JA20 rotor at 15,000 rpm. The cleared lysate was then filtered through a 0.45 μm Millipore membrane and loaded onto a Whatman DE52 anion exchange column (1.6 × 50 cm), preequilibrated in 10 mM Tris, 50 mM NaCl (pH 8).

The column was washed thoroughly with loading buffer, after which a linear gradient from 50 to 250 mM NaCl in 10 mM Tris (pH 8) was applied over a total volume of 400 ml. Active fractions were pooled, concentrated to 0.8 ml in an Amicon ultrafiltration cell using a PM10 membrane, and applied to a prepacked Sephacryl 300 HR 16/60 gel filtration column (AP Biotech). Elution was in 10 mM Tris, 360 mM NaCl (pH 8) by gravity flow (5.2 ml/hr). The pooled active fractions were concentrated and buffer-exchanged into 10 mM citrate, 50 mM NaCl (pH 5.4) by ultrafiltration. This resulted in a precipitate, which was removed by centrifugation; the activity remained in the supernatant. The gel filtration step was then repeated using 10 mM citrate, 50 mM NaCl (pH 5.4) as the buffer and the eluent peak containing the activity was collected.

Assay for Enzyme Activity

Cyanide concentrations were determined using a modification of the picric acid method (Fisher and Brown, 1952). 20 μl of potassium cyanide stock ([KCN] = 25 mM, [Tris-HCl] = 125 mM [pH 8]) was added to an equal volume of sample and incubated at 37°C for 30 min. The samples were then placed on ice and added to 80 μl of a solution containing 0.5% (w/v) picric acid, 0.25 M Na_2CO_3. The resulting solutions were boiled for 5 min and diluted to 1 ml with H_2O. The color change was determined by measuring the absorbance at 520 nm. One unit of activity was defined as the degradation of 1 μm of cyanide per minute.

Electron Microscopy

The purified enzyme was diluted 1:40 in 10 mM triethanolamine, 50 mM NaCl (pH 8) to a final protein concentration 0.3 mg/ml. A carbon-coated copper grid was placed on a droplet of this enzyme preparation for 10 min, blotted, and then stained with 2% uranyl acetate for 3 min. The grid was then blotted and air dried.

Micrographs were taken using the minimum dose technique at the 50,000× magnification setting on a JEOL 1200EXII at an underfocus of 0.1–0.7 μm. Fifteen images were digitized on a Leafscan 45 linear CCD scanner (Ilford Ltd, Cheshire, UK) with a step size of 20 μm, which corresponds to a pixel size of 4.0 Å on the specimen. The pixel size was confirmed after the reconstruction by plotting the correlation coefficient of the fit of the dimer model to the map at a single location as a function of pixel size. Particle selection was performed with Ximdisp (Crowther et al., 1996). A total of 7008 particles were selected in 80 × 80 pixel areas, band pass filtered between 250–15 Å without CTF correction, and normalized to the same mean and standard deviation. These and all subsequent image processing steps were carried out with SPIDER (Frank et al., 1996).

Three-Dimensional Reconstruction

The images were classified into 84 classes using the method of Penczek et al. (1996). Membership of these classes was refined by several cycles of multireference alignment (Joyeux and Penczek, 2002) and the exclusion of poorly matching images. The angular

relationship of the 49 most populous classes was determined by a common lines-based method (Penczek et al., 1996). A starting model was created by the iterative 3D reconstruction method of Penczek et al. (1992) according to these angular relationships. Projections of the starting model were then made using a set of 84 quasi equally spaced projection directions, spanning an entire hemisphere with a step size of 15° to produce a set of reference images. Multiple cycles of refinement comprising (1) multireference alignment, (2) averaging the sets of images determined to match each projection, (3) 3D reconstruction (Penczek et al., 1992) of the averages by the iterative method to create a model, and (4) reprojecting this model to create the next generation of reference images were performed. After 47 cycles it became apparent by visual inspection that the structure had a global 2-fold axis. The orientation of the 2-fold axis was determined and the model was rotated so that the 2-fold axis was located along the x axis . In 17 subsequent cycles of refinement, 2-fold averaging was performed. The procedure was terminated when no further changes in the map were visible. The resolution was determined by dividing the images into two equally populated sets, reconstructing separately and determining the Fourier shell correlation (Harauz and van Heel, 1986) in shells of one pixel thickness.

Sequence Alignment and Model Building

Searching and alignments based on structural homology were done with GenTHREADER (Jones, 1999a). Structural alignments of Nit and DCase were done with ALIGN (Cohen, 1997). Amino acid substitution was done with SCWRL (Bower et al., 1997) based on these alignments. Dimers coupled at either the A or B surface were generated by superimposing the model structure on the appropriate chains of the Nit domain. Dimer models having the deletions but lacking the insertions were docked into the density using the contour based low resolution program (CoLoRes) in the SITUS package (Chacón and Wriggers, 2002) and the results of the docking were inspected with O (Jones et al., 1991). Ribbon diagrams were made with MOLSCRIPT (Kraulis, 1991) and rendered with RASTER3D (Merritt and Bacon, 1997). The molecular envelope was drawn with CONSCRIPT (Lawrence and Bourke, 2000).

Supplemental Data

Supplemental data, including the class averages and movies showing the evolution of the map and the fit of the dimer model to the map, may be found on *Structure*'s web site (http://www.structure.org/cgi/content/full/11/11/1413/DC1).

The map has been deposited in the Electron Microscopy Database and has accession code EMD-1050.

Acknowledgments

We thank Helen Saibil, Christine Slingsby, and Brendon Price for their critical reading of drafts of the manuscript. B.T.S. and M.N.B. are grateful for assistance received from Elena Orlova, Mohamed Jaffer, James Duncan, Dennis Burford, Michael Lawrence, and Brendon Price. We gratefully acknowledge support from the Wellcome Trust, Birkbeck College, the Robert A. Welch Foundation, the University of Houston Environmental Institute, and the Gulf Coast Hazardous Substance Research Center # 069UHH0789. M.N.B. received financial assistance from the National Research Foundation.

Received: October 23, 2002
Revised: June 26, 2003
Accepted: July 3, 2003
Published: November 4, 2003

References

Almatawah, Q.A., Cramp, R., and Cowan, D.A. (1999). Characterization of an inducible nitrilase from a thermophilic bacillus. Extremophiles *3*, 283–291.

Bartling, D., Seedorf, M., Schmidt, R.C., and Weiler, E.W. (1994). Molecular characterization of two cloned nitrilases from *Arabidopsis thaliana*: key enzymes in biosynthesis of the plant hormone indole-3-acetic acid. Proc. Natl. Acad. Sci. USA *91*, 6021–6025.

Bhalla, T., Miura, A., Wakamoto, A., Ohba, Y., and Furuhashi, K. (1992). Asymmetric hydrolysis of α-aminonitrilase to optically active amino acids by a nitrilase of *Rhodococcus rhodochrous* PA-34. Appl. Microbiol. Biotechnol. *37*, 184–190.

Bower, M., Cohen, F.E., and Dunbrack, R.L., Jr. (1997). Sidechain prediction from a backbone-dependent rotamer library: a new tool for homology modeling. J. Mol. Biol. *267*, 1268–1282.

Brenner, C. (2002). Catalysis in the nitrilase superfamily. Curr. Opin. Struct. Biol. *12*, 775–782.

Chacón, P., and Wriggers, W. (2002). Multi-resolution contour-based fitting of macromolecular structures. J. Mol. Biol. *317*, 375–384.

Cluness, M.J., Turner, P.D., Clements, E., Brown, D.T., and O'Reilly, C. (1993). Purification and properties of cyanide hydratase from *Fusarium lateritium* and analysis of the corresponding *chyl* gene. J. Gen. Microbiol. *139*, 1807–1815.

Cohen, G.H. (1997). *ALIGN:* a program to superimpose protein coordinates, accounting for insertions and deletions. J. Appl. Crystallogr. *30*, 1160–1161.

Cowan, D., Cramp, R., Pereira, R., Graham, D., and Almatawah, Q. (1998). Biochemistry and biotechnology of mesophilic and thermophilic nitrile metabolizing enzymes. Extremophiles *2*, 207–216.

Crowther, R.A., Henderson, R., and Smith, J.M. (1996). MRC image processing programs. J. Struct. Biol. *116*, 9–16.

Fisher, F., and Brown, J.S. (1952). Colorimetric determination of cyanide in stack gas and waste water. Anal. Chem. *24*, 1440–1444.

Frank, J., Radermacher, M., Penczek, P., Zhu, J., Li, Y., Ladjadj, M., and Leith, A. (1996). SPIDER and WEB: Processing and visualization of images in 3D electron microscopy and related fields. J. Struct. Biol. *116*, 190–199.

Fry, W.E., and Munch, D.C. (1975). Hydrogen cyanide detoxification by *Gloeocercospora sorghi*. Physiol. Plant Path. *7*, 23–33.

Goldlust, A., and Bohak, Z. (1989). Induction, purification, and characterization of the nitrilase of *Fusarium oxysporum* f. sp. *melonis*. Biotechnol. Appl. Biochem. *11*, 581–601.

Harauz, G., and van Heel, M. (1986). Exact filters for general geometry three-dimensional reconstruction. Optik *73*, 146–156.

Harper, D.B. (1976). Purification and properties of an unusual nitrilase from *Nocardia* N.C.I.B. 11216. Biochem. Soc. Trans. *4*, 502–504.

Harper, D.B. (1977). Microbial metabolism of aromatic nitriles. Enzymology of C-N cleavage by *Nocardia* sp. (*Rhodochrous* group) N.C.I.B. 11216. Biochem. J. *165*, 309–319.

Ingvorsen, K., Højer-Pedersen, B., and Godtfredsen, S.E. (1991). Novel cyanide hydrolysing enzyme from *Alcaligenes xylosxidans* subsp. *denitrificans*. Appl. Environ. Microbiol. *57*, 1783–1789.

Jandhyala, D., Berman, M., Meyers, P.R., Sewell, B.T., Willson, R.T., and Benedik, M.J. (2003). CynD, the Cyanide Dihydratase from *Bacillus pumilus:* gene cloning and structural studies. Appl. Environ. Microbiol. *69*, 4794–4805.

Jones, D.T. (1999a). GenTHREADER: an efficient and reliable protein fold recognition method for genomic sequences. J. Mol. Biol. *287*, 797–815.

Jones, D.T. (1999b). Protein secondary structure prediction based on position-specific scoring matrices. J. Mol. Biol. *292*, 195–202.

Jones, T.A., Zou, J.Y., Cowan, S.W., and Kjeldgaard, M. (1991). Improved methods for binding protein models in electron density maps and the location of errors in these models. Acta Crystallogr. *A47*, 110–119.

Joyeux, L., and Penczek, P.A. (2002). Efficiency of 2D alignment methods. Ultramicroscopy *92*, 33–46.

Kobayashi, M., Yanaka, N., Nagasawa, T., and Yamada, H. (1990). Purification and characterization of a novel nitrilase of *Rhodococcus rhodochrous* K22 that acts on aliphatic nitriles. J. Bacteriol. *172*, 4807–4815.

Kobayashi, M., Yanaka, N., Nagasawa, T., and Yamada, H. (1992). Primary structure of an aliphatic nitrile-degrading enzyme, aliphatic nitrilase, from *Rhodococcus rhodochrous* K22 and expression of its gene and identification of its active site residue. Biochemistry *31*, 9000–9007.

Kraulis, P.J. (1991). MOLSCRIPT: A program to produce both detailed and schematic plots of protein structures. J. Appl. Crystallogr. *24*, 946–950.

Lawrence, M.C., and Bourke, P. (2000). A program for generating electron density isosurfaces (an alternative to the usual chicken-wire). J. Appl. Crystallogr. *33*, 990–991.

Merritt, E.A., and Bacon, D.J. (1997). Raster3D: Photorealistic molecular graphics. Meth. Enzymol. *277*, 505–524.

Meyers, P., Rawlings, D.E., Woods, D.R., and Lindsey, G.G. (1993). Isolation and characterization of a cyanide dihydratase from *Bacillus pumilus* C1. J. Bact. *175*, 6105–6112.

Mizuguchi, K., Deane, C.M., Blundell, T.L., Johnson, M.S., and Overington, J.P. (1998). JOY: protein sequence-structure representation and analysis. Bioinformatics *14*, 617–623.

Nagasawa, T., and Yamada, H. (1989). Microbial transformations of nitriles. Trends Biotechnol. *7*, 153–158.

Nagasawa, T., Wieser, M., Nakamura, T., Iwahara, N., Yoshida, T., and Gekko, K. (2000). Nitrilase of *Rhodococcus rhodochrous* J1—conversion into the active form by subunit association. Eur. J. Biochem. *267*, 138–144.

Nakai, T., Hasgawa, T., Yamashita, E., Yamamoto, M., Kamasuka, T., Ueki, T., Nanba, H., Ikenaka, Y., Takahashi, S., Sato, M., et al. (2000). Crystal structure of N-carbamyl-D-amino acid amidohydrolase with a novel catalytic framework common to amidohydrolases. Structure *8*, 729–737.

Pace, H.C., Hodawadekar, S.C., Draganescu, A., Huang, J., Bieganowski, P., Pekarsky, Y., Croce, C.M., and Brenner, C. (2000). Crystal structure of the worm NitFhit Rosetta Stone protein reveals a Nit tetramer binding two Fhit dimers. Curr. Biol. *10*, 907–917.

Pace, H.C., and Brenner, C. (2001). The nitrilase superfamily: classification, structure and function. Genome Biology *2*, reviews0001.1–0001.9.

Penczek, P., Rademacher, M., and Frank, J. (1992). Three-dimensional reconstruction of single particles embedded in ice. Ultramicroscopy *40*, 33–53.

Penczek, P., Zhu, J., and Frank, J. (1996). A common-lines based method for determining orientations for N>3 particle projections simultaneously. Ultramicroscopy *63*, 205–218.

Price, B., Chang, P., Jandhyala, D.M., Benedik, M., and Sewell, B.T. (2002). The quaternary structure of *Gloeocercospora sorghi* nitrilase (cyanide hydratase) as revealed by negative staining. 15th International Congress on Electron Microscopy, Durban, 565–566.

Rockel, B., Peters, J., Kühlmorgen, B., Glaeser, R.M., and Baumeister, W. (2002). A giant protease with a twist: the TPP II complex from *Drosophila* studied by electron microscopy. EMBO J. *21*, 5979–5984.

Stalker, D.M., Malyj, L.D., and McBride, K.E. (1988). Purification and properties of a nitrilase specific for the herbicide bromoxynil and corresponding nucleotide sequence analysis of the *bxn* gene. J. Biol. Chem. *263*, 6310–6314.

Stevenson, D.E., Feng, R., Dumas, F., Groleau, D., Mihoc, A., and Storer, A.C. (1992). Mechanistic and structural studies on *Rhodococcus* ATCC 39484 nitrilase. Biotechnol. Appl. Biochem. *15*, 283–302.

Wang, P., Matthews, D.E., and Van Etten, H.D. (1992). Purification and characterization of cyanide hydratase from the phytopathogenic fungus *Gloeocercospora sorghi*. Arch. Biochem. Biophys. *298*, 569–575.

Watanabe, A., Yano, K., Ikebukuro, K., and Karube, I. (1998a). Cloning and expression of a gene encoding cyanidase from *Pseudomonas stutzeri* AK61. Appl. Microbiol. Biotechnol. *50*, 93–97.

Watanabe, A., Yano, K., Ikebukuro, K., and Karube, I. (1998b). Cyanide hydrolysis in a cyanide-degrading bacterium, *Pseudomonas stutzeri* AK61, by cyanidase. Microbiol. *144*, 1677–1682.

Yamamoto, K., and Komatsu, K. (1991). Purification and characterization of nitrilase responsible for the enantioselective hydrolysis from *Acinetobacter* sp. AK 226. Agric. Biol. Chem. *55*, 1459–1466.

Accession Numbers

The map has been deposited in the Electron Microscopy Database and has accession code EMD-1050.